Azimuthal AVO analysis with anisotropic spreading correction: A synthetic study

XIAOXIA XU and ILYA TSVANKIN, Center for Wave Phenomena, Colorado School of Mines, Golden, USA

Analysis of prestack amplitude variation with offset and azimuth (often called "azimuthal AVO analysis" or "AVAZ") is one of the most effective tools for seismic characterization of fractures and in-situ stress field. The main advantage of amplitude methods compared to traveltime inversion is their high vertical resolution that makes AVO analysis applicable to relatively thin reservoirs. Also, body-wave amplitudes are highly sensitive to seismic anisotropy and, in particular, to azimuthal velocity variations associated with vertical fracture systems and nonhydrostatic stresses.

Similar to traveltimes, reflection amplitudes recorded at the surface represent effective quantities influenced by the medium properties along the whole raypath. The goal of AVO analysis is to resolve the local physical parameters at the reservoir level using the reflection coefficient, which is hidden in the measured amplitude.Therefore, a critical element of AVO processing is separation of the reflection coefficient from the source signature and the propagation factors, most notably from the geometrical spreading in the overburden.

In practice, it is often assumed that as long as the overburden is structurally simple (e.g., layer-cake), it should not produce substantial amplitude distortions. This "common-sense" assumption, however, can be dangerously misleading if some of the overburden formations are anisotropic. Anisotropy above the reflector acts like a lens that focuses and defocuses seismic energy in accordance with angular velocity variations. In his book, Tsvankin (2005) gives striking examples of weakly anisotropic VTI (transversely isotropic with a vertical symmetry axis) models that produce dramatic amplitude variations along the wavefronts of both P- and S-waves. If not corrected for, this strong angle dependence of the anisotropic geometrical-spreading factor can compromise the AVO signature (e.g., the AVO gradient) and lead to erroneous interpretation results.

In particular, the AVO response for wide-azimuth data can be distorted by the azimuthal variation of geometrical spreading caused by aligned vertical fractures in the overburden (fractures often permeate much of the section above the reservoir). Still, most anisotropic AVO algorithms employ empirical amplitude corrections used in isotropic processing (e.g., the t- or t^2-gain factors). Such approximate amplitude treatment generally does not prevent azimuthal AVO from estimating the dominant fracture directions, as attested by successful case studies reported in the literature (e.g., Hall and Kendall, 2003; Gray and Todorovic-Marinic, 2004). However, to put the method on a firm quantitative footing and make it suitable for estimating the physical properties of fractures, one has to apply a more robust geometrical-spreading correction that honors the azimuthal anisotropy in the overburden.

In principle, the geometrical-spreading factor can be computed using dynamic ray tracing or other forward-modeling techniques. Unfortunately, our anisotropic velocity models are rarely accurate enough to make this approach practical. Therefore, we recently proposed a *moveout-based* anisotropic spreading-correction method that can be abbreviated as "MASC." This method makes it possible to compute geometrical spreading for wide-angle reflections in horizontally layered, azimuthally anisotropic media directly from the reflection traveltimes. The spreading correction is preceded by 3D nonhyperbolic moveout analysis using the semblance algorithm of Vasconcelos and Tsvankin (2006). The moveout parameters estimated from wide-azimuth data serve as the input to the geometrical-spreading correction. MASC does not require knowledge of the velocity model (except for the velocities in the layer containing the sources and receivers) and was shown to be sufficiently robust in the presence of noise.

Here, we process full-waveform 3D synthetic reflection data to answer several important practical questions regarding MASC and anisotropic spreading correction for PP-waves:

1) Can MASC, despite its reliance on ray theory, accurately reconstruct reflection coefficients in the presence of strong azimuthal anisotropy?
2) Can we replace MASC with simple gain corrections commonly used in practice?
3) Is it possible to ignore the contribution of the transmission coefficients (which are not included in MASC) along the raypath?

Table 1. *Parameters of a three-layer medium used in the numerical tests (model 1).*

	Layer 1	Layer 2	Layer 3
Symmetry type	ISO	ORTH	ISO
Thickness (km)	0.5	1.0	∞
Density (g/cm^3)	2.1	2.1	2.12
V_{P0} (km/s)	2.1	2.2	2.3
V_{S0} (km/s)	1.05	1.1	1.15
$\varepsilon^{(1)}$	0	0.317	0
$\delta^{(1)}$	0	-0.054	0
$\gamma^{(1)}$	0	0.513	0
$\varepsilon^{(2)}$	0	0.121	0
$\delta^{(2)}$	0	0.046	0
$\gamma^{(2)}$	0	0.138	0
$\delta^{(3)}$	0	0.1	0
$\eta^{(1)}$	0	0.42	0
$\eta^{(2)}$	0	0.07	0
$\eta^{(3)}$	0	0.05	0

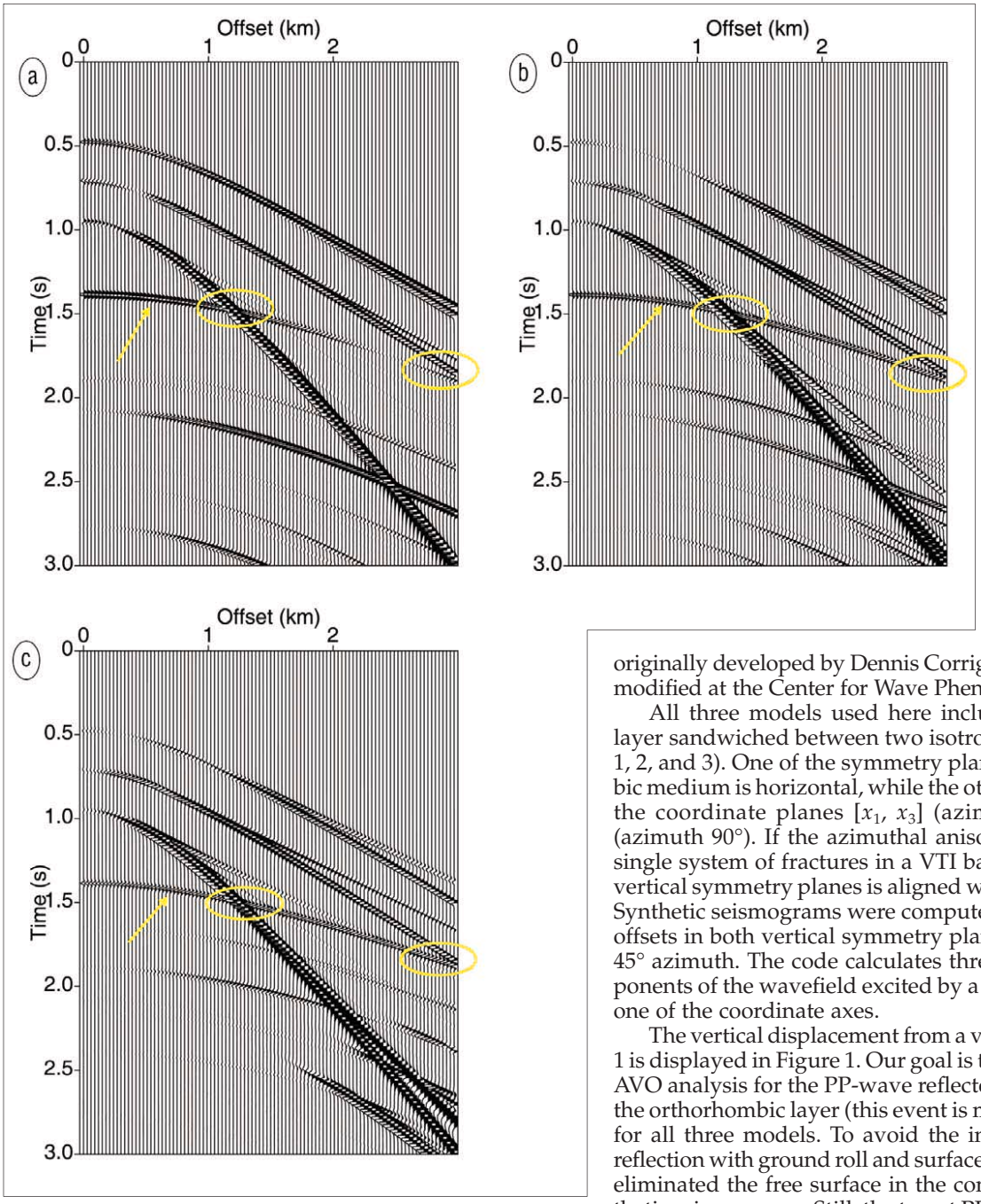

Figure 1. Synthetic shot gathers for model 1 (Table 1) computed by the reflectivity method in three azimuthal directions: (a) 0° (symmetry plane [x_1, x_3]); (b) 45°; and (c) 90° (symmetry plane [x_2, x_3]). The arrows mark the target PP-wave reflected from the bottom of the orthorhombic layer. The ellipses highlight the areas of interference of the target PP event with the PS and SS reflections from the top of the orthorhombic layer.

We begin by describing the modeling code and the algorithm used to reconstruct the reflection coefficient from the picked amplitudes of reflected PP-waves. Then we compare the performance of MASC and empirical gain corrections for three relatively simple models that include an orthorhombic layer beneath an isotropic overburden. Although most current implementations of azimuthal AVO analysis operate with HTI (TI with a horizontal symmetry axis) media, orthorhombic symmetry is more typical for realistic fractured reservoirs. Recent work of Grechka and Kachanov (2006) shows that orthorhombic models accurately describe even multiple sets of vertical fractures with arbitrary azimuthal orientations.

Synthetic modeling. The modeling algorithm, based on the anisotropic version of the reflectivity method, is designed to simulate exact 3D wavefields for horizontally layered, anisotropic media. The reflectivity code (ANISYNPA) was originally developed by Dennis Corrigan at ARCO and later modified at the Center for Wave Phenomena.

All three models used here include an orthorhombic layer sandwiched between two isotropic media (see Tables 1, 2, and 3). One of the symmetry planes of the orthorhombic medium is horizontal, while the other two coincide with the coordinate planes [x_1, x_3] (azimuth 0°) and [x_2, x_3] (azimuth 90°). If the azimuthal anisotropy is caused by a single system of fractures in a VTI background, one of the vertical symmetry planes is aligned with the fracture strike. Synthetic seismograms were computed for a wide range of offsets in both vertical symmetry planes, as well as for the 45° azimuth. The code calculates three displacement components of the wavefield excited by a point force parallel to one of the coordinate axes.

The vertical displacement from a vertical force for model 1 is displayed in Figure 1. Our goal is to carry out azimuthal AVO analysis for the PP-wave reflected from the bottom of the orthorhombic layer (this event is marked by the arrows) for all three models. To avoid the interference of this PP reflection with ground roll and surface-related multiples, we eliminated the free surface in the computation of the synthetic seismograms. Still, the target PP event interferes with the PS- and SS-wave reflections from the top of the orthorhombic layer, particularly for model 3 (Figure 2), which causes distortions of the picked AVO response.

Estimation of the reflection coefficient from the AVO response. MASC computes the offset- and azimuth-dependent geometrical-spreading factor for a given reflection event using the zero-offset time t_0 and effective moveout parameters $V_{nmo}^{(1)}$, $V_{nmo}^{(2)}$, $\eta^{(1)}$, $\eta^{(2)}$, and $\eta^{(3)}$. The symmetry-plane normal-moveout (NMO) velocities $V_{nmo}^{(1)}$ and $V_{nmo}^{(2)}$ determine the NMO ellipse on conventional spreads, while $\eta^{(1)}$, $\eta^{(2)}$, and $\eta^{(3)}$ are the anellipticity parameters (they are similar to the well-known parameter η for VTI media) responsible for nonhyperbolic (long-spread) moveout. The moveout parameters are estimated with a global semblance algorithm that maximizes semblance computed for all offsets and azimuths in the gather. It should be emphasized that the geometrical-spreading correction is not influenced

Table 2. Parameters of model 2. Model 1 was modified to reduce the azimuthal variation of the reflection coefficient while keeping the geometrical-spreading factor unchanged.

	Layer 1	Layer 2	Layer 3
Symmetry type	ISO	ORTH	ISO
Thickness (km)	0.5	1.0	∞
Density (g/cm^3)	2.1	2.1	2.12
V_{P0} (km/s)	2.1	2.2	2.3
V_{S0} (km/s)	1.05	1.1	1.15
$\varepsilon^{(1)}$	0	0.317	0
$\delta^{(1)}$	0	-0.054	0
$\gamma^{(1)}$	0	0.138	0
$\varepsilon^{(2)}$	0	0.121	0
$\delta^{(2)}$	0	0.046	0
$\gamma^{(2)}$	0	0.03	0
$\delta^{(3)}$	0	0.1	0
$\eta^{(1)}$	0	0.42	0
$\eta^{(2)}$	0	0.07	0
$\eta^{(3)}$	0	0.05	0

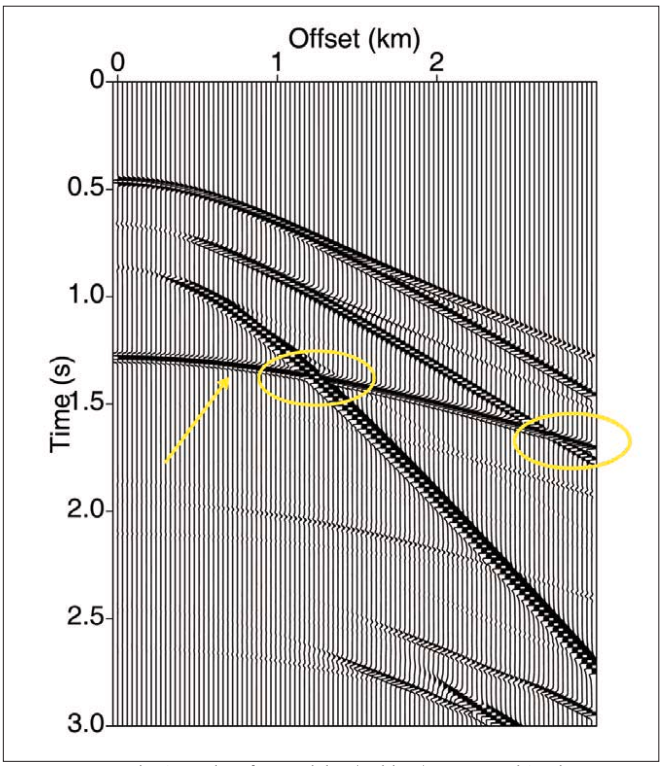

Figure 2. *Synthetic gather for model 3 (Table 3) computed in the symmetry plane [x_2, x_3] (azimuth 90°).*

by the tradeoffs between the NMO velocities and η-parameters, as long as the reconstructed moveout function is sufficiently close to the actual traveltimes.

The processing flow starts with picking raw amplitudes of a certain event on all traces along the traveltime surface defined by the estimated moveout parameters. Then the picked amplitudes are corrected for the anisotropic geometrical spreading computed for each offset and azimuth. Finally, assuming that the sources and receivers are located in an isotropic layer with a known P-wave velocity, the algorithm removes the source and receiver directivity factors using local time slopes (i.e., horizontal slownesses) calculated from the moveout function.

Since our models are nonattenuative, the corrected amplitude should be determined primarily by the plane-wave reflection coefficient. The only propagation factor not accounted for in this algorithm is the product of the transmission coefficients along the raypath, which is usually close to a constant (see below). A scalar related to the strength of the source can be removed by simple normalization.

The output amplitudes have to be smoothed to mitigate the distortions caused by the interference of the PP reflection with shear and converted waves (see the ellipses in Figures 1 and 2).The smoothing was accomplished by least-squares fitting of a fourth-order polynomial in the horizontal slowness to the reconstructed reflection coefficients. In practice, the results of AVO processing often require smoothing because of noisy amplitudes, variations in the source and receiver coupling, etc.

Model 1. The parameters of the orthorhombic layer in model 1 (see Table 1) are based on Wang's (2002) results for two transversely isotropic brine-saturated shale samples. Orthorhombic symmetry can be fully described by the two vertical velocities (V_{P0} for P-waves and V_{S0} for one of the split S-waves) and seven anisotropy parameters ($\varepsilon^{(1)}$, $\varepsilon^{(2)}$, $\delta^{(1)}$, $\delta^{(2)}$, $\delta^{(3)}$, $\gamma^{(1)}$, and $\gamma^{(2)}$). The anellipticity parameters $\eta^{(1)}$, $\eta^{(2)}$, and $\eta^{(3)}$ control P-wave nonhyperbolic moveout. For a detailed explanation, see Tsvankin (2005). The main reason for choosing this model is that the large difference between the SH-wave parameters $\gamma^{(1)}$ and $\gamma^{(2)}$ causes an extremely pronounced azimuthal variation of the P-wave AVO gradient. Note that $\gamma^{(1)} = 0.513$ is much higher than the average value of Thomsen's γ for shales (0.2), so this model likely exaggerates the typical magnitude of the azimuthal AVO response.

The PP-wave reflection coefficient from the bottom of the orthorhombic layer reconstructed by our moveout-based geometrical-spreading correction and by the empirical t^2 gain is marked by dashed lines in Figures 3a and 3b. (We chose the t^2 function because it generally gives better results for our models than the linear t compensation or Newman's correction.) For comparison, Figure 3 also displays the exact reflection coefficient (solid lines). To remove the source factor, the estimated reflection coefficient is normalized to match the exact value at normal incidence (zero offset).

The maximum horizontal slowness (0.3 s/km) in Figure 3 corresponds to an incidence angle at the source close to 40° (it varies with azimuth) and an offset-to-depth-ratio slightly larger than two. The slownesses up to 0.15 s/km (the corresponding incidence angle is up to 20°) define what we will call the near-offset amplitude response; the reflection coefficient in this slowness range is governed mostly by the AVO gradient.

Clearly, for near offsets the MASC algorithm recovers the reflection coefficient with extremely high accuracy (Figure 3a). The small deviation of the estimated reflection coefficient from the exact curve at far offsets for azimuths of 45° and 90° is related to the interference with shear and mode-converted waves (Figures 1b and 1c). The excellent agreement between the reconstructed and exact reflection

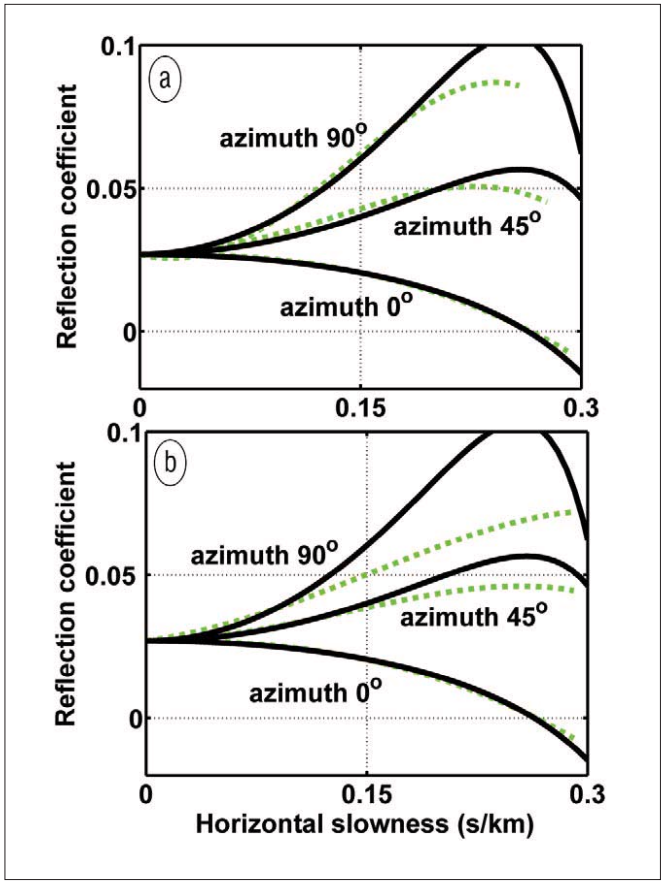

Figure 3. Comparison of the reconstructed (dashed lines) and exact (solid lines) reflection coefficients for the PP-wave reflected from the bottom of the orthorhombic layer in model 1. The reflection coefficient is estimated using (a) MASC; and (b) the t^2 gain. The offset-to-depth ratio that corresponds to the maximum horizontal slowness (0.3 s/km) is slightly larger than two.

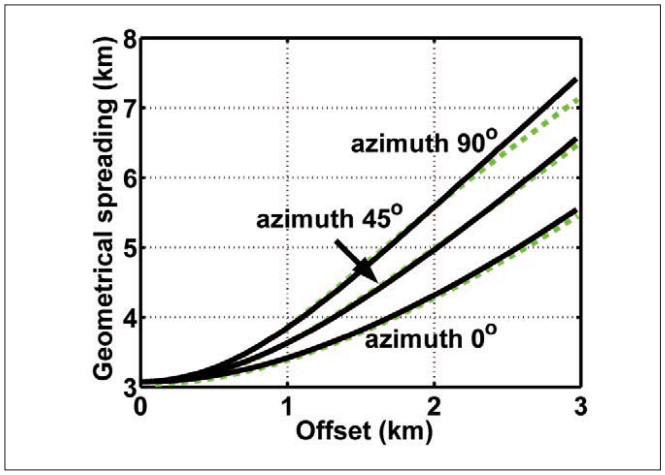

Figure 4. Comparison of the geometrical spreading computed by MASC (dashed lines) and dynamic ray tracing (solid) for the PP reflection from the bottom of the orthorhombic layer in model 1.

coefficients for a wide range of offsets and azimuths is ensured by the application of the moveout-based geometrical-spreading correction. Figure 4 confirms that the output of MASC for all three azimuths practically coincides with the geometrical spreading computed by dynamic raytracing.

The performance of the simple t^2 gain correction often used in practice varies with azimuth (Figure 3b). For an azimuth of 0° the estimated reflection coefficient is close to the exact value for the full offset range. The accuracy of the t^2 gain, however, is much lower for the other two azimuths, especially at far offsets.

Since the traveltime depends on both polar and azimuthal velocity variations, the t^2 function absorbs some of the influence of the anisotropy on the geometrical-spreading factor. For that reason, the t^2 gain happens to be adequate for the 0° azimuth, although it does not accurately reproduce the variation of the spreading away from that direction. Still, it is clear from Figure 3b that the error of the t^2 correction does not seriously compromise qualitative analysis of the AVO gradient as a function of azimuth. For model 1, the variation of the AVO gradient between the symmetry planes is so pronounced that the geometrical-spreading factor does not have to be computed with high accuracy. Quantitative inversion of the AVO response on long-spread gathers, however, should be based on the MASC algorithm.

Table 3. *Parameters of model 3. The orthorhombic layer corresponds to the "standard" orthorhombic model of Schoenberg and Helbig (1997).*

	Layer 1	Layer 2	Layer 3
Symmetry type	ISO	ORTH	ISO
Thickness (km)	0.5	1.0	∞
Density (g/cm^3)	2.44	2.70	2.44
V_{P0} (km/s)	2.16	2.437	2.16
V_{S0} (km/s)	1.150	1.265	1.150
$\varepsilon^{(1)}$	0	0.329	0
$\delta^{(1)}$	0	0.083	0
$\gamma^{(1)}$	0	0.046	0
$\varepsilon^{(2)}$	0	0.258	0
$\delta^{(2)}$	0	-0.078	0
$\gamma^{(2)}$	0	0.182	0
$\delta^{(3)}$	0	-0.106	0
$\eta^{(1)}$	0	0.211	0
$\eta^{(2)}$	0	0.398	0
$\eta^{(3)}$	0	0.194	0

Model 2. The second model is designed in such a way that the geometrical spreading of the target event from the bottom of the orthorhombic layer is the same as that in model 1, but the azimuthal variation of the reflection coefficient is much less pronounced (which is more typical for field data). The ratio of the overall azimuthal variation of the geometrical spreading and that of the reflection coefficient (estimated at a horizontal slowness of 0.15 s/km) for model 2 reaches 40%. In the absence of interference with other arrivals at large offsets, the reflection coefficient recovered by MASC is almost identical to the exact value for the whole range of offsets and azimuths (Figure 5a).

The impact of the errors produced by the t^2 gain in this model is amplified by the relatively weak azimuthal dependence of the reflection coefficient (Figure 5b). The reflection coefficients after the t^2 gain are close for all three azimuths (and practically coincide for 45° and 90°, even at far offsets).

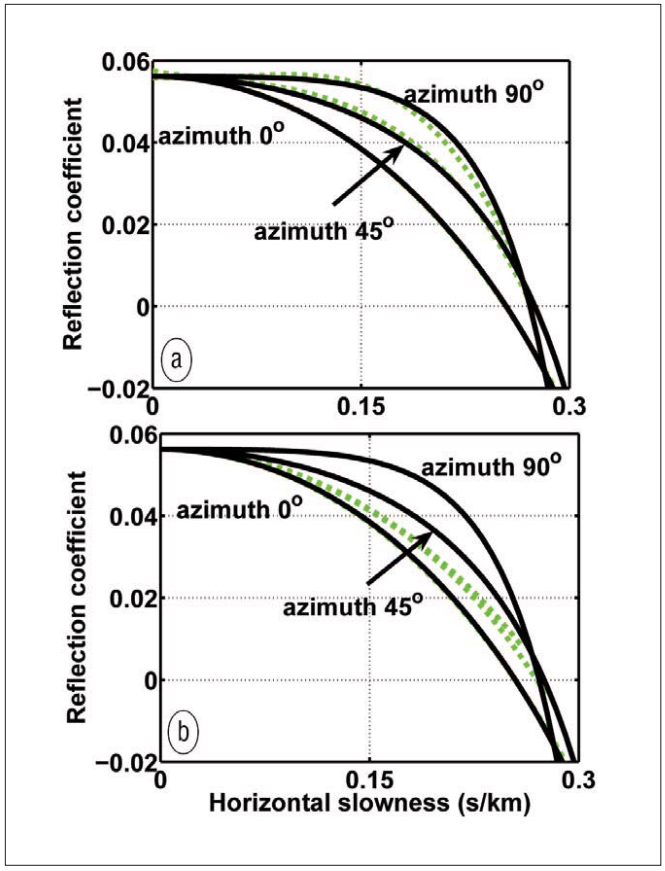

Figure 5. Comparison of the reconstructed (dashed lines) and exact (solid) reflection coefficients for model 2. The reflection coefficient is estimated using (a) MASC; and (b) the t^2 gain. The reconstructed reflection coefficients for the 45° and 90° azimuths on plot (b) practically coincide with one another; for the 0° azimuth, the reconstructed coefficient is almost invisible because it is close to the exact value. The offset-to-depth ratio that corresponds to the maximum horizontal slowness (0.3 s/km) is close to two.

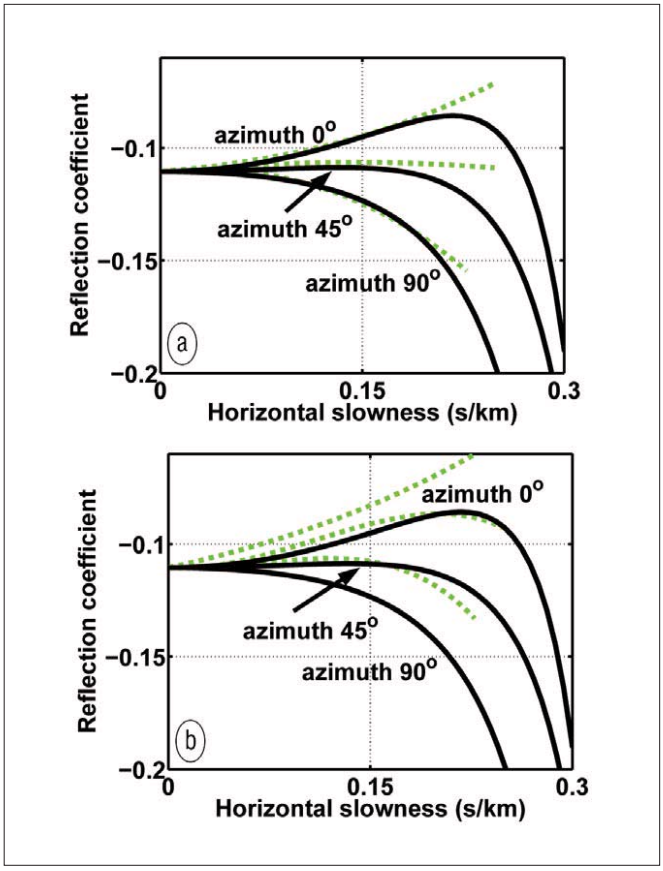

Figure 6. Comparison of the reconstructed (dashed lines) and exact (solid) reflection coefficients for model 3. The reflection coefficient is estimated using (a) MASC; and (b) the t^2 gain. The offset-to-depth ratio that corresponds to the maximum horizontal slowness (0.3 s/km) is close to 2.5.

Evidently, such small azimuthal differences in amplitude would be undetectable in the presence of realistic noise. Hence, application of the empirical t^2 correction for this model obliterates the azimuthal AVO signature and makes it useless for fracture-detection purposes.

Model 3. The parameters of the orthorhombic layer in model 3 are typical for a set of parallel, vertical, penny-shaped cracks embedded in a VTI background medium (the so-called "standard orthorhombic model" of Schoenberg and Helbig). The PP reflection coefficient from the bottom of the orthorhombic layer computed by MASC remains accurate up to a horizontal slowness of about 0.2 s/km (Figure 6a). For larger slownesses (i.e., at far offsets) the reconstructed reflection coefficient is severely distorted by the interference of the target event with the PS conversion from the top of the orthorhombic layer (see Figure 2). Note that for model 3 the slowness 0.15 s/km corresponds to an incidence angle close to 25° (slightly higher than that for model 1) and an offset-to-depth ratio of one.

The t^2 gain correction for this model works better than for model 2 but worse than for model 1 (Figure 6b). The ratio of the overall azimuthal variation of the geometrical spreading and that of the reflection coefficient, estimated at a horizontal slowness of 0.15 s/km, for model 3 is 15%. For all three azimuths, the reflection coefficient after the t^2 correction is larger than the exact value and the error becomes noticeable at relatively small offsets. The reconstructed reflection coefficient in the 90° direction even has the sign of the AVO gradient wrong. However, while the t^2 gain is clearly inadequate for purposes of quantitative AVO inversion, it correctly reproduces the azimuthal trend of the AVO gradient between the vertical symmetry planes.

Influence of the transmission loss. The transmission coefficients along the raypath are not part of the geometrical-spreading correction and are difficult to estimate from surface data. To evaluate the transmission loss for our models, we subtract from unity the product of the transmission coefficients along the raypath of the target PP reflection (Figure 7). For all three models, the transmission loss becomes noticeable only at far offsets, but the related azimuthal amplitude variation is substantially smaller than that of the reflection coefficient (as can be seen by comparing Figure 7a with the solid curves in Figure 3). Therefore, the transmission loss can be considered a secondary factor in azimuthal AVO analysis, which is confirmed by the high accuracy of MASC in our examples.

Discussion. Our modeling results show that application of MASC is essential if the azimuthal variation of the geometrical spreading is not negligible compared to that of the reflection coefficient. It is important to keep in mind that geometrical spreading and reflection coefficient are governed by two different sets of medium parameters defined at different scales. When the model is orthorhombic, the

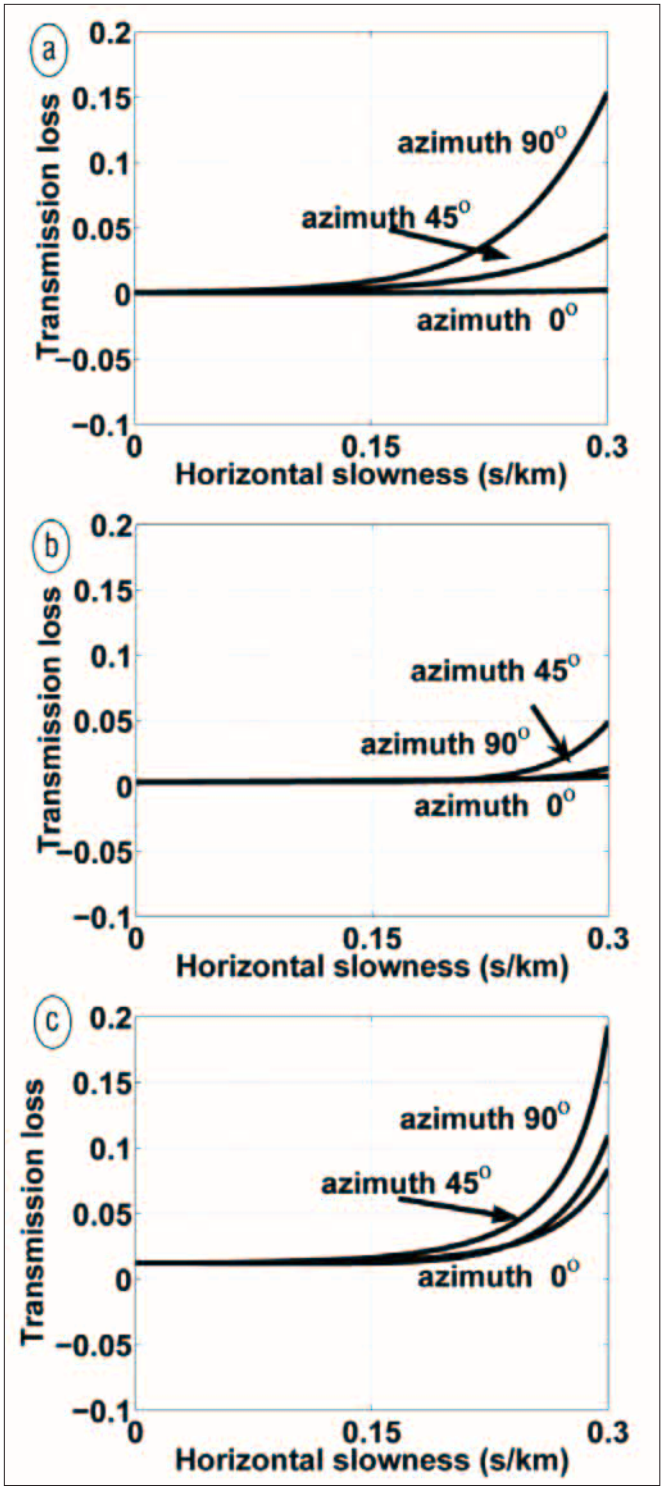

Figure 7. *Transmission loss for the PP reflection from the bottom of the orthorhombic layer in (a) model 1; (b) model 2; and (c) model 3. The loss is computed by subtracting from unity the product of the plane-wave transmission coefficients along the raypath.*

azimuthal variation of the P-wave AVO gradient is controlled by the *local* jump in the shear-wave splitting parameter and in the difference between the Thomsen δ parameters ($\delta^{(2)} - \delta^{(1)}$) across the target interface. In contrast, geometrical spreading of reflected waves depends on the *effective* (average) parameters of the overburden.

If fracturing is largely limited to reservoir formation, the azimuthal amplitude variation of the reflection from the top of the reservoir generally follows the reflection coeffi-

cient (the case of our model 1). This explains why the results of azimuthal AVO analysis with the conventional (isotropic) spreading correction often are in good agreement with other fracture-characterization methods. However, natural fractures that respond to the local stress field often permeate the whole section and lead to substantial azimuthal anisotropy in the overburden. In such cases, application of MASC is highly beneficial even for purposes of "qualitative" AVO analysis designed to estimate the relative change in the AVO response between the symmetry planes. Also, the azimuthal variation of geometrical spreading is more significant for the reflection from the *bottom* of the reservoir, especially for relatively thick reservoir layers. Note that the moveout and geometrical spreading of reflections from beneath the reservoir contain useful information for reservoir characterization which is complementary to that provided by the reflection coefficient.

Long-offset reflection data used in our synthetic study help to increase the sensitivity of the azimuthal AVO response to the anisotropy parameters. However, even if amplitude analysis is restricted to the AVO gradient estimated on conventional offsets, the geometrical-spreading correction can benefit from nonhyperbolic moveout inversion for the anellipticity parameters $\eta^{(1,\,2)}$. Although this result seems counterintuitive, it is explained by the strong dependence of geometrical spreading on the second traveltime derivative with respect to offset.

Conclusions. The transformation of seismic amplitudes measured at the surface into the reflection coefficient at the target horizon is a critically important step in AVO analysis. Here, we tested the moveout-based anisotropic geometrical-spreading correction (MASC) on long-offset, wide-azimuth synthetic data from three models which included a strongly anisotropic layer of orthorhombic symmetry. The results show that although MASC is based on ray theory, it accurately reconstructs the azimuthally varying reflection coefficient for a wide range of offsets and azimuths. The errors in the estimated reflection coefficient are mostly caused by interference-related amplitude distortions.

In practice, azimuthal AVO analysis often involves an empirical gain correction designed to compensate for the amplitude loss in the overburden. Our tests demonstrate that although the t^2 gain absorbs some of the influence of anisotropy on geometrical spreading, it produces significant errors in the reflection coefficient, especially for offsets-to-depth ratios greater than unity. Therefore, the empirical correction cannot be used in quantitative inversion of the azimuthally varying AVO response for the anisotropy parameters (e.g., for the fracture compliances).

On the other hand, most existing applications of azimuthal AVO are limited to estimating the principal azimuthal directions of the AVO gradient and its variation between the vertical symmetry planes. This relative azimuthal change in the AVO gradient measured over a fractured reservoir is then used to identify "sweet spots" of high fracture density. For models where the azimuthal variation of the reflection coefficient is much more pronounced than that of geometrical spreading (e.g., our models 1 and 3), the t^2 gain is sufficient to reproduce the general azimuthal trend of the reflection coefficient.

However, as the ratio of the overall azimuthal variation of the geometrical spreading and that of the reflection coefficient (estimated for an incidence angle of about 20°) increases to 40% in model 2, the empirical correction completely smears the AVO signature. For model 2, the reflection coefficient after the t^2 gain is so weakly dependent on azimuth that it contains almost no information about the reservoir. On the whole, application of MASC becomes essential even in qualitative AVO analysis when the azimuthal variation of the geometrical spreading reaches about one-third of that of the reflection coefficient.

It should be emphasized that the MASC algorithm can be conveniently incorporated into the processing flow prior to velocity model-building at almost no extra cost. Indeed, azimuthal AVO analysis always is preceded by a moveout correction designed to flatten the event of interest. The estimated effective moveout parameters can then be used as the input to the MASC algorithm, which does not require any other information about the velocity model (other than the layer that contains the sources and receivers).

Suggested reading. The theory and algorithm of the moveout-based anisotropic spreading correction (MASC) method are described in "Geometrical spreading of P-waves in horizontally layered, azimuthally anisotropic media" by Xu et al. (GEOPHYSICS, 2005) and "Anisotropic geometrical-spreading correction for wide-azimuth P-wave reflections" by Xu and Tsvankin (GEOPHYSICS, 2006). "Nonhyperbolic moveout inversion of wide-azimuth P-wave data for orthorhombic media" by Vasconcelos and Tsvankin (*Geophysical Prospecting*, 2006) introduces the moveout-inversion algorithm applied prior to the geometrical-spreading correction. A detailed discussion of body-wave amplitudes and geometrical spreading in anisotropic media can be found in the book *Seismic Signatures and Analysis of Reflection Data in Anisotropic Media* by Tsvankin (Elsevier, 2005). The book also explains the notation for orthorhombic media used in this article. The anisotropy parameters for models 1 and 2 are based on the laboratory measurements in "Seismic anisotropy in sedimentary rocks, part 2: Laboratory data" by Wang (GEOPHYSICS, 2002). The parameters for model 3 are computed for the "standard" fractured orthorhombic medium introduced in "Orthorhombic media: Modeling elastic wave behavior in a vertically fractured earth" by Schoenberg and Helbig (GEOPHYSICS, 1997). Effective orthorhombic models for multiple fracture sets are discussed in the paper "Seismic characterization of multiple fracture sets: Does orthotropy suffice?" by Grechka and Kachanov (GEOPHYSICS, 2006). *Reflection Coefficients and Azimuthal AVO Analysis in Anisotropic Media* by Rüger (SEG, 2001) gives a comprehensive and clear exposition of AVO equations for anisotropic media. For a concise description of the main concepts of azimuthal AVO analysis, see "Using AVO for fracture detection: Analytic basis and practical solutions" by Rüger and Tsvankin (*TLE*, 1997). Recent case studies of azimuthal AVO analysis are presented in "Fracture detection using 3D azimuthal AVO" by Gray and Todorovic-Marinic (CSEG *Recorder*, 2004) and "Fracture characterization at Valhall: Application of P-wave amplitude variation with offset and azimuth (AVOA) analysis to a 3D ocean-bottom data set" by Hall and Kendall (GEOPHYSICS, 2003). TLE

Acknowledgments: We are grateful to Ken Larner, Rodrigo Fuck, and Yaping Zhu (all of CSM) for useful suggestions. Dave Hale (CSM), Andreas Rüger (Landmark Graphics), and Debashish Sarkar (GX Technology, formerly CSM) helped us to improve reflectivity code ANISYNPA. The exact reflection coefficients were computed using software written by Petr Jílek (BP, formerly CSM). The support for this work was provided by the Consortium Project on Seismic Inverse Methods for Complex Structures at the Center for Wave Phenomena and by the Chemical Sciences, Geosciences and Biosciences Division, Office of Basic Energy Sciences, Office of Science, U.S. Department of Energy.

Corresponding authors: Xiaoxia Xu (xiaoxia@dix.mines.edu) and Ilya Tsvankin (ilya@dix.mines.edu)